

Analysis of 3D-Printed Auxetic Lattice Structures for Robotic Skin Applications

Beom Jun Kim¹ and John Meshinsky¹

Abstract—This project evaluates the suitability of beam-based auxetic lattices, manufactured from thermoplastic polyurethane (TPU), as candidates for robotic skin. Auxetic structures are structures that have the property of a negative Poisson’s ratio, where an increase in height also increases the material’s contraction, which is key to energy absorption, low stiffness, and flexibility, making them attractive for protective interfaces and impact mitigation [1][2][3]. We numerically compare three lattice topologies – a conventional triangular lattice, a re-entrant “bowtie” lattice, and a star-shaped lattice – using a 2D beam-based discrete elastic model. For each lattice panel, we simulate vertical compression by fixing the top row of nodes and applying an upward or downward force to the bottom row. From the nodal trajectories, we extract the global height and a center-row width to characterize local auxetic behavior. These measurements are used to compute longitudinal strain, transverse strain, and an effective Poisson’s ratio over time. The triangular lattice shows unstable and sign-changing Poisson’s ratio and limited auxetic response. In contrast, the bowtie lattice develops strong negative Poisson’s ratio values (down to about 1.4) but is prone to necking and collapse in the central region. We identify numerical and modeling limitations – including nodal overlap, missing contact forces, and a linear-elastic material model – and outline design and simulation improvements needed before experimental 3D-printed skins can be reliably evaluated, particularly in light of the strain-stiffening behavior of real TPU [14].

I. INTRODUCTION

This mechanical protective layer, or this robotic “skin”, for mechanical devices such as exoskeletons and humanoid robots must protect the underlying structure while accommodating large deformations and joint rotations. Conventional solid TPU covers, although mechanically robust and easy to fabricate [4], often behave like stiff torsional springs that resist bending and compressive deformation. These can act as a source of resistance to the motion of the robotic joint, leading to a large sim2real gap. Auxetic materials, characterized by a negative Poisson’s ratio, offer an alternative approach by expanding laterally when stretched and contracting laterally when compressed [8]. This unusual kinematic response has been shown to enhance indentation resistance [2] and vibration damping [3][6], both of which are desirable for protective skins and impact-mitigating layers. Recent work has demonstrated that 3D-printed TPU lattice architectures enable designers to tune effective stiffness and deformation behavior by selecting unit-cell topology and relative density [4][5][7]. Auxetic lattices have been explored for protective layers [1], vibration and shock absorption [6][7],

soft actuators and robotic skins [9][12], and resistive tactile sensors [11]. For example, bowtie-shaped unit cells have been observed to have large negative Poisson’s ratios and recoverable strain when printed in TPU [5][7][9][10]. In this project, our goal was to design and experimentally validate 3D-printed auxetic skins for covering a soft exoskeleton or a humanoid limb. These skins should (i) exhibit auxetic characteristics and (ii) provide impact and shock mitigation. As a first step toward this goal, the present study focuses on numerical simulations of planar lattices subjected to longitudinal compression. In this report, we address the following specific questions: How do an auxetic triangular lattice, an inverted hexagon or “bow-tie”, and a star-shaped lattice compare in their deformation patterns, effective Poisson’s ratio, and energy absorption under vertical tension and compression?

What are the limitations of simulation in terms of calculations in our current beam-based framework that lead to unrealistic behavior of collapse, and how do these limitations inform future experimental design?

By answering these questions, we aim to narrow down suitable unit-cell candidates and clarify the simulation improvements required for reliable design of robotic skins.

II. METHODOLOGY

1. Lattice Structure Creation

The simulation creates a network of discrete elastic rods in two dimensions to model the nature and behaviour of these lattice structures under applied load. The forces calculated using the equations of motion follow a discrete-rod framework with contributions from axial and bending energies. Time integration is performed using an implicit Newton–Raphson update, which improves stability under large deformations and is employed for 2D auxetic foam simulations [13].

A. Lattice geometry and material model

First, the lattices needed to be created for testing. All lattices are modeled as networks of Euler–Bernoulli beam elements connecting mass points (nodes), similar in spirit to prior lattice and auxetic-foam simulations [4][5][13]. The creation function uses parameters for length, nodes per beam, and lattice size to generate each lattice, ensuring a consistent measure of lattice structure for comparison. The geometry is generated procedurally: first, the shape of the first unit cell is modeled; then, the cell is repeated to match the lattice size; and finally, the repeated pattern cells are connected

¹Authors are graduate student of Mechanical and Aerospace Engineering, University of California Los Angeles, 405 Hilgard Avenue, United States of America

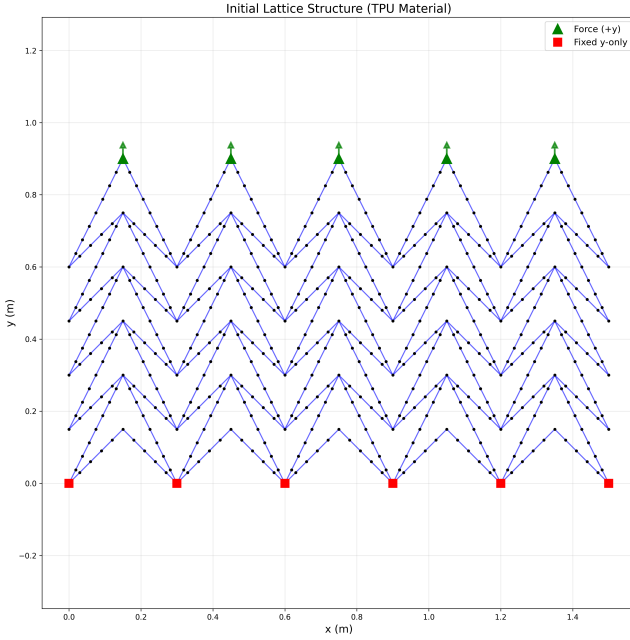


Fig. 1. Initial structure of a triangle lattice

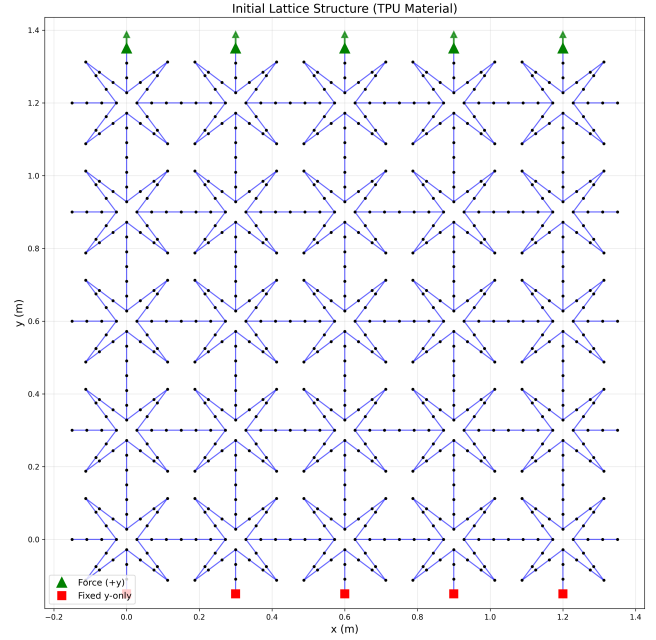


Fig. 2. Initial structure of a Star-Grid lattice

to form the lattice, allowing the same framework to be reused for multiple topologies. Triangular lattice: A periodic chevron lattice made of repeated V-shaped segments, forming alternating peaks and valleys across the structure.(Figure 1).

B. Boundary conditions and loading

To mimic a skin patch attached to a rigid frame, the nodes are fully constrained, all on the bottom row in both the x-axis and y-axis:n The free degrees of freedom on the top row allow for the system to spread to cause little interference to the width deformation of the system. The nodes on the top row remain free to move, but to a uniform vertical load pointing upward (tensile from the model's viewpoint). The load is constantly applied in time.

$$F_y(t) = 200.00$$

The intermediate rows have no prescribed displacements and move in response to the internal beam forces and the applied loads at the top nodes, putting the system in tension. The total simulated time is 0.35 seconds with time steps of 0.001s, which is sufficient for the system to reach a quasi-static configuration at each sampled time instant. The total time was measured from testing to provide insight into the behavior before it becomes excessive.

C. Measurement definitions

From the nodal positions, we define several geometric measures used to compute strain and Poisson's ratio.

1) *Global Height and Width*: The lattices are measured by using their changing height and width throughout the simulation. This is calculated by using the maximum and minimum y-axis and x-axis values, respectively, to see the deformation of the whole lattice structure over time, to be used in further analysis of the properties of the structure.

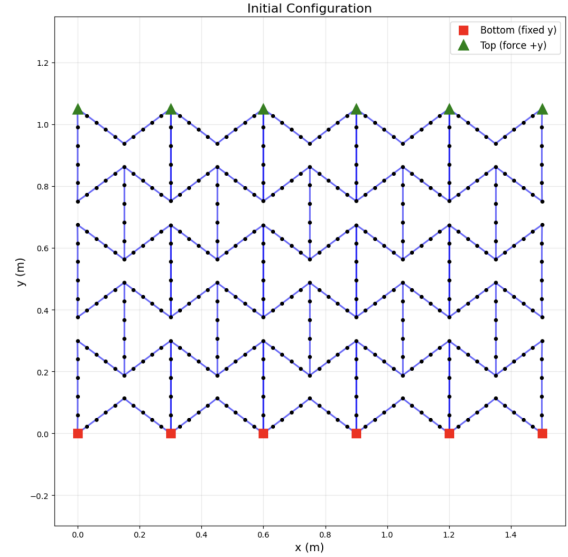


Fig. 3. Initial structure of a Bow-Tie lattice

2) *Effective Strain and Poisson's ratio*.: The effective longitudinal and transverse strains were computed from the global height and width of the lattice, defined as the difference between the maximum and minimum nodal coordinates in the loading (y) and transverse (x) directions, respectively: This measurement will be used to determine the evolution of Poisson's ratio and to track changes in the lattice structure. The Poisson's ratio compared with the displacements will give more insight into how the lattice structure responds to the loads over time.

The longitudinal (vertical) strain based on global height is

$$\varepsilon_y(t) = \frac{H(t) - H_0}{H_0}$$

and the transverse strain is defined as

$$\varepsilon_x(t) = \frac{W(t) - W_0}{W_0}$$

The effective Poisson's ratio is then

$$\nu(t) = -\frac{\varepsilon_x(t)}{\varepsilon_y(t)}$$

For an ideal auxetic material under compression, $\varepsilon_y < 0$ and $\varepsilon_x < 0$, yielding $\nu < 0$. We monitor $\varepsilon_y(t)$, $\varepsilon_x(t)$, and $\nu(t)$ throughout the simulation to compare the two lattice designs.

3) *Energy used:* To measure the energy used to cause displacement on the lattice structure, the work done on the system to cause deformation compares how the energy is being absorbed by the system, and gives an idea of the relative stiffness of the structure under a load. The more work done, the more energy it absorbs. The higher the work done, the more it represents the relative stiffness of the structure, as it shows its deformation more under a lower force load.

4) *Scale of Lattice:* In our testing, we found that larger-scale lattice models perform better in our simulation than smaller-scale models. This might be due to the limitations of simulations, and a larger scale provides higher resolution to observe the model's behavior in a more stable environment. For our purposes as well, the scale of the properties does not matter in the comparison of our value between the different lattice structures, so we favored the stability of our model for behavior over how close our scale is to the intended model.

III. RESULTS AND DISCUSSION

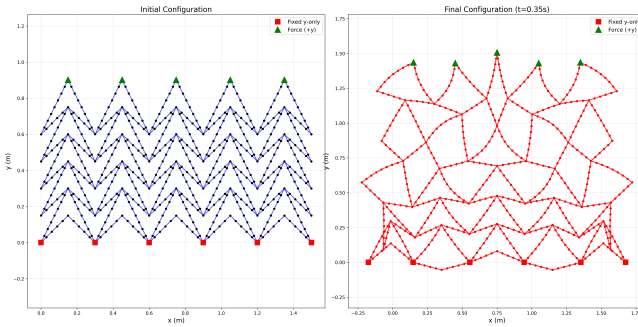


Fig. 4. Comparison between initial and final state of the triangle lattice

A. Triangular lattice under Tension

Figure 7 shows the time evolution of the triangular lattice. The initial configuration forms a nearly uniform triangular grid. As the top row moves upward, the structure first deforms smoothly. As it deforms, the triangular shape spreads along its width, causing the structure to expand, with increasing width deformation accompanying increasing height deformation. The global width and height curves (Figure 10) reveal transverse expansion followed by its contraction. The longitudinal strain, ε_y , reaches approximately 75% at

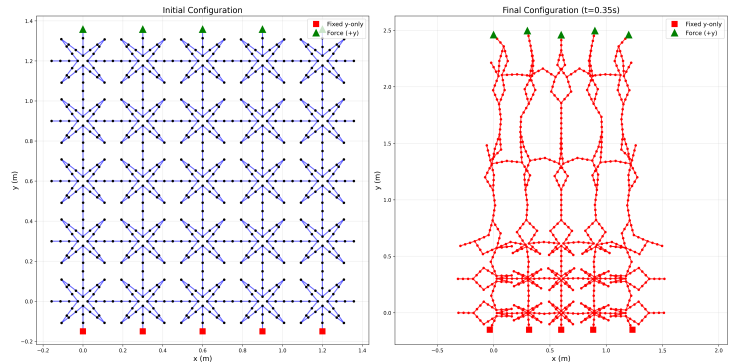


Fig. 5. Comparison between initial and final state of the Star-Grid lattice

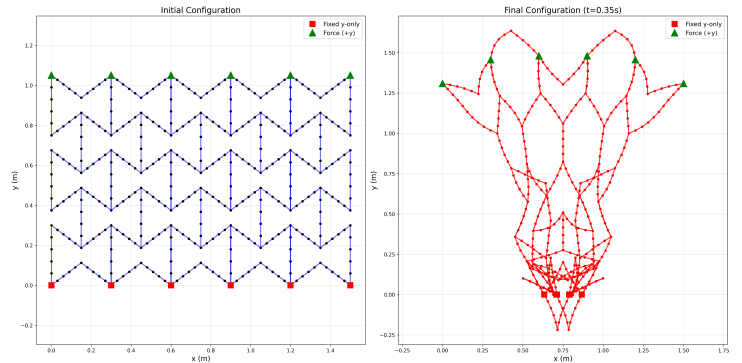


Fig. 6. Comparison between initial and final state of the Bow-Tie lattice

the end of the simulation, while the transverse strain, ε_x , seems to increase at a slightly faster rate than the ε_y , but begins to decrease a bit over time. As a result, the effective Poisson's ratio drops below a maximum of -2.5 while starting to reduce at a slower rate than when it was increasing. This behavior demonstrates that the triangular lattice exhibits a stable auxetic response under tension. The structure undergoes steady deformation in both width and height. The work on the system over time, as seen in the structure of the model, can be seen in Figure 13. This indicates that the work of 139 J is moderate in comparison to the other models, but it can absorb shock reasonably well and exhibits moderate stiffness.

B. Star-Grid lattice under Tension

For observation of the star-grid pattern, Figure 8 illustrates the time evolution of the Star-Grid lattice. Initially, the structure consists of a nearly uniform grid of beams interconnected by star-shaped nodes. As the top row rises, the upper portion of the lattice rapidly deforms. This deformation causes the top row to expand laterally, resulting in a gradual widening of the structure as its height increases. This process demonstrates a simultaneous increase in both width and height deformation. The global width and height curves exhibit interesting deformation in the simulation. The longitudinal strain, ε_y , reaches approximately 75% at the end of the simulation, while the transverse strain, ε_x , seems to increase at a slower rate than the ε_y . As a result,

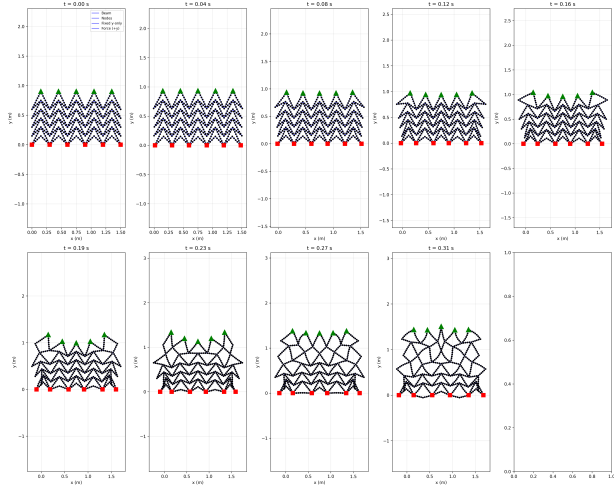


Fig. 7. Time evolution of a triangle lattice structure shape during actuation.

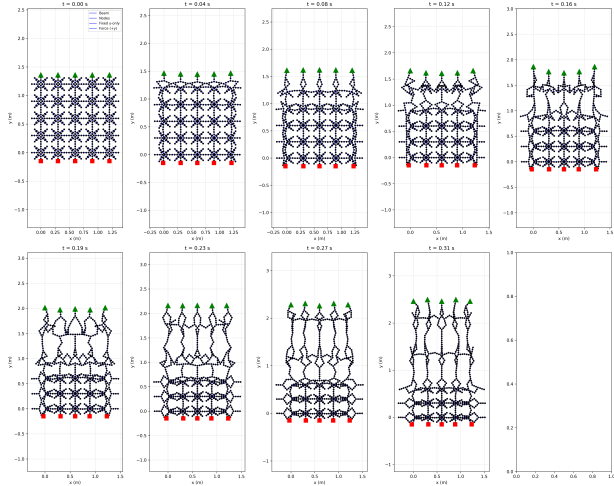


Fig. 8. Time evolution of a Star-Grid lattice structure shape during actuation.

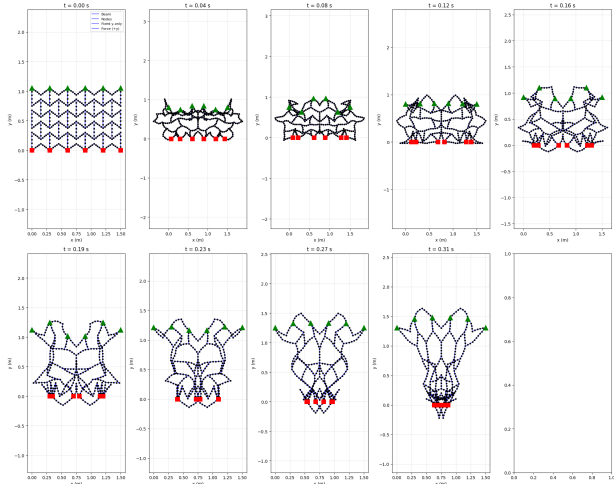


Fig. 9. Time evolution of a Bow-Tie lattice(case1) structure shape during actuation.

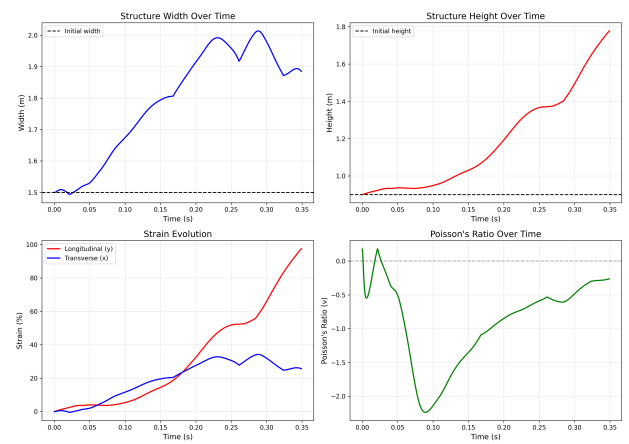


Fig. 10. Time evolution of a triangle lattice structure dimensions, strain, and effective Poisson's ratio during actuation.

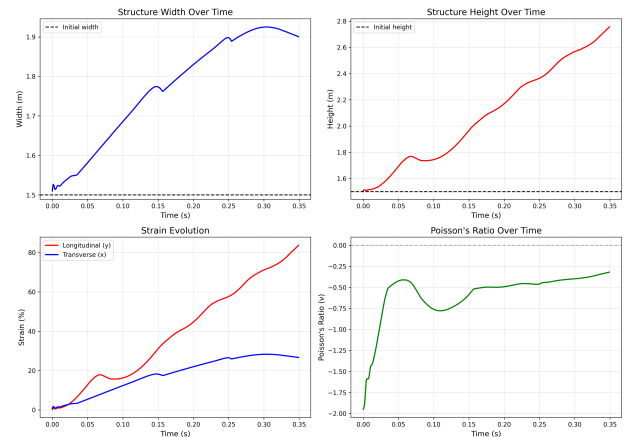


Fig. 11. Time evolution of a Star-Grid lattice structure dimensions, strain, and effective Poisson's ratio during actuation.

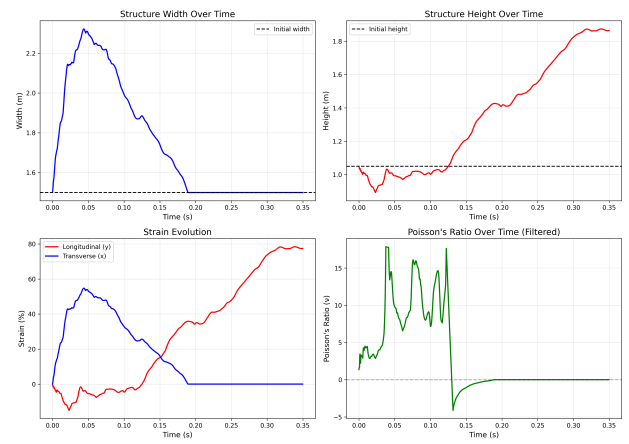


Fig. 12. Time evolution of a Bow-Tie dimensions, strain, and effective Poisson's ratio during actuation.

effective Poisson's ratio drops below a maximum of -2.0 while oscillating after that point. This behavior demonstrates that the Star-Grid lattice exhibits a stable auxetic response under tension, characterized by steady height deformation and slower width deformation. The work performed on the system over time, as illustrated in Figure 14, totals 249 J—more than double that observed for the triangular lattice. This suggests that the Star-Grid lattice absorbs shock effectively and possesses significantly lower stiffness compared to the triangular lattice.

C. Bowtie lattice under tension

Two numerical experiments were performed on the same bow-tie auxetic lattice after observing unexpected behavior from the initial case: The first case is under the same parameters as the other lattice structures for comparison.

A testing case, a large lattice with 15x15 unit cells, subjected to compressive loading.

The first case under the initial parameters had experienced an unusual stiffness in comparison to the other lattice structures, which the bending and stretching forces overcame the initial applied force and showed negative work done, as well as displayed a positive effective Poisson Ratio. Even with greater magnitudes of force applied, it seemed the lattice structure had still overcome the applied force. To observe the behavior of the negative Poisson ratio, a second case was run using different parameters in our efforts to observe the behavior. For observation of the bow-tie lattice (Case 1), Figure 9 illustrates the time evolution of the global strains and effective Poisson's ratio. As the vertical load is applied, the structure develops a localized “necking” region near the center of the lattice, where the bow-tie cells open laterally while the overall height changes only slightly. This deformation mode leads to a gradual and pronounced increase in the global width, whereas the total height experiences only a modest shortening. The global strain curves show that the longitudinal strain, ε_y , remains relatively small and compressive starting, reaching about 10%, to gradually increase to 79% by the end of the simulation. In contrast, the transverse strain, ε_x , increases monotonically up to nearly +50% before dropping back down to 0%. Because ε_y steadily increases while ε_x grows, the effective Poisson's ratio, $-\varepsilon_x/\varepsilon_y$, starts as positive and attains values between approximately 6 and 17 under this shocked state. This indicates that, at the global scale, the bow-tie lattice does not initially exhibit an auxetic response until about 0.13 seconds into the simulation. It initially behaves as a highly laterally compliant but non-auxetic structure, becoming wider as it is compressed in the loading direction. This initial behavior may be due to high stiffness forces inherent in the structure itself: the applied force along the y-axis is resisted by forces within the structure, whereas the transverse x-axis responds to the applied force, resulting in the increased width deformation. The work history in Figure 15 shows an increase in the magnitude of negative work, reaching a max about -60 J before switching to positive work finishing at 71 J. The negative sign arises from the chosen sign convention, so the

magnitude of this quantity represents the mechanical energy absorbed by the lattice during deformation. Compared to more compliant auxetic configurations, the total absorbed energy is smaller, suggesting that the bow-tie lattice in this loading case is relatively stiffer and concentrates deformation in a localized region rather than distributing it uniformly throughout the structure. It seems that the stiffness of the structure caused it to run unstable with the initial parameters briefly at the start. In case 2, the large-lattice compressive case, exhibited an effective negative Poisson's ratio, whereas the initial case did not. In Figure 16, a negative Poisson ratio was observed in this case; however, under the compressive force, the model quickly becomes unstable without the force values. This is also an example of how in the current model, it does not handle compressive forces or at smaller scales. This helped to observe the negative Poisson ratio, but also helped to recognize the issues with the model at smaller scales.

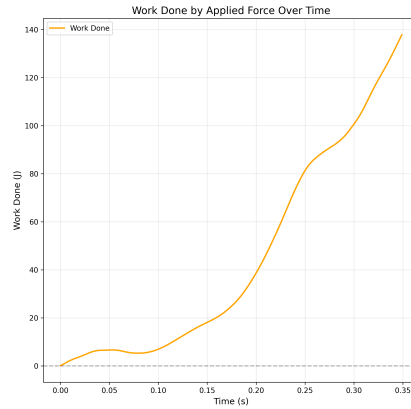


Fig. 13. Work done by applied force over time (triangle lattice structure)

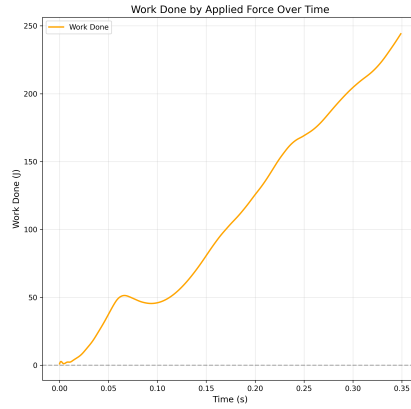


Fig. 14. Work done by applied force over time (Star-Grid lattice structure)

D. Quantitative comparison

The triangular lattice achieves only moderate negative Poisson's ratio values. In contrast, the bowtie lattice produces a consistently negative Poisson's ratio once necking initiates, with a magnitude significantly larger than typical re-entrant

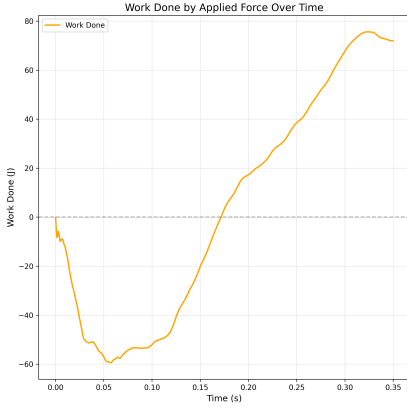


Fig. 15. Work done by applied force over time (Bow-Tie lattice structure)

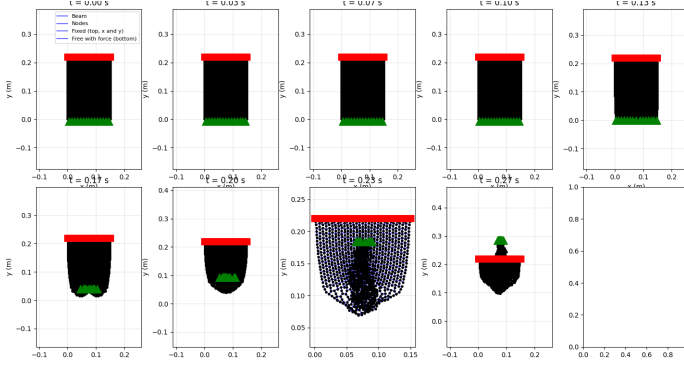


Fig. 16. Time evolution of a Bow-Tie lattice(case2) structure shape during actuation.

foams reported in the literature (often in the range 0.2 to 1.0 under moderate strain [2,6–8]). This suggests that our beam-based bowtie model may be overly compliant in the joints or missing stabilizing contact interactions that would limit the collapse in a real printed TPU structure.

E. Relation to prior work

Studies on 3D-printed auxetic TPU lattices report that these re-entrant and bowtie-type geometries can maintain structural stability under relatively large compressive strains while providing a smooth negative Poisson’s ratio response [4,5,7,9,10]. Our simulated bowtie lattice successfully reproduces the strong auxetic trend but predicts more severe necking and a higher magnitude of ν than typically observed. One likely reason is our use of a linear elastic material model with constant $E=26\text{ MPa}$. Real TPU exhibits pronounced strain-stiffening: its tangent modulus increases with axial stretch, especially at large strains [14]. In the current model, the stiffness remains low even as the unit cells fold, allowing the center region to collapse more deeply than a physical specimen would. Incorporating a hyperelastic or strain-dependent modulus model should restrain this runaway collapse and produce a more realistic plateau in the stress-strain response.

F. Numerical limitations

Beyond material modeling, several numerical and geometric limitations affect our results:

1) Nodal overlap and missing contact.: Nodes and beams are treated as dimensionless entities, so different parts of the lattice can pass through each other. When this happens, the solver resolves the overlap via extremely large internal forces, which can drive rapid collapse or unrealistic oscillations. A robust self-contact model is needed to prevent interpenetration and to approximate the finite thickness of the printed struts, similar to the considerations in tiled auxetic cylinders for soft robots [12].

2) Low stiffness at joints.: Because each beam is connected via idealized pins or compliant joints, some nodes act as nearly frictionless hinges. Under compression, these joints can rotate too freely, producing large rotations at low energy cost. This effect artificially enhances the auxetic response and contributes to the very high negative Poisson’s ratios; related hinge-dominated failure mechanisms have also been noted in beam-based auxetic models [7]. Introducing rotational springs or stiffening the joints would better match real printed connections. However, it seems that this limitation is greatly reduced at the larger scale models on which we run our simulations.

3) Geometric irregularities from procedural generation.: Small inconsistencies in beam length or node spacing lead to inhomogeneous stiffness. Regions with shorter beams or denser connectivity become artificially stiff, while sparse regions are more flexible. This spatial variation can bias where necking initiates and how the collapse pattern develops.

4) Time-integration: Although an implicit scheme is used, the combination of stiff beams and strong collision forces (when overlaps occur) can still challenge convergence. Additional damping or adaptive time-stepping, as used in other numerical studies of auxetic foams [13], may be required when implementing a more sophisticated contact model. These limitations explain why the bowtie lattice in simulation undergoes dramatic necking and why the triangular lattice shows complex, sometimes oscillatory width changes instead of a clean macroscopic auxetic response.

IV. CONCLUSION AND FUTURE WORK

In this project, we numerically investigated two auxetic lattice designs – a conventional triangular network and a re-entrant bowtie lattice – as potential candidates for 3D-printed robotic skin. Using a beam-based nodal model with implicit time integration, we compressed panels of each lattice between a fixed top boundary and a loaded bottom boundary, then extracted longitudinal and transverse strains to compute an effective Poisson’s ratio. Our main findings are:

The triangular lattice provides limited and unstable auxetic behavior. Its effective Poisson’s ratio changes sign and reaches both large positive and moderate negative values as localized buckling modes develop. This lack of consistency makes it a poor candidate for a predictable robotic skin layer.

The bowtie lattice shows strong auxetic behavior with local Poisson’s ratios near 1.4 under high compression, inspiring confidence in its potential for robotic skin applications.

Several modeling and numerical limitations, like linear elasticity and missing contact, likely exaggerate collapse, prompting the audience to consider the need for further refinement.

For future work, we propose the following directions:

A. Hyperelastic material model.

Implement a strain-dependent or hyperelastic constitutive law for TPU, informed by uniaxial test data and prior characterization of strain-stiffening in TPU [14], to capture modulus evolution with strain and limit unrealistic folding. This will provide more realistic behavior for producing these lattice structures for robotic skin.

B. Contact and finite thickness.

Introduce self-collision detection and penalty or constraint-based contact forces so that beams cannot pass through each other. This will regularize collapse behavior and improve the validity of Poisson's ratio measurements at high strain. These functions are more helpful in compression analysis.

C. Joint stiffening and geometric refinement.

Add rotational springs at junctions and refine the procedural geometry to ensure uniform beam lengths and cell sizes. This should reduce the door-hinge effect and produce more homogeneous deformation, making the numerical results more comparable to experimental bowtie skins [5,7,9,10].

D. Experimental validation.

Fabricate triangular and bowtie panels using 3D-printed TPU and perform compression tests to measure global and local Poisson's ratio, stiffness, and energy absorption, following methodologies used in [4,5,9]. Comparing these results with the improved simulations will validate the model and guide further design iterations.

E. Integration with robotic hardware.

Once a robust skin design is identified, mount it on a simplified limb or exoskeleton segment to assess how auxetic behavior influences comfort, joint range of motion, and impact mitigation in a realistic setting, inspired by applications in soft actuators and tactile skins [9,11,12]. Overall, the study demonstrates that re-entrant auxetic lattices show promise for robotic skin applications and highlights the importance of accurate material modeling and contact mechanics. The refined simulation framework and insights from this work will support the next stage of designing and testing 3D-printed auxetic skins for wearable robotics.

REFERENCES

- [1] Y. Wang et al., "Auxetic composite laminates with through-thickness negative Poisson's ratio: Low-velocity impact behaviors," *Polymers*, 2022.
- [2] O. Duncan et al., "Effect of Poisson's ratio on the indentation of open-cell foam," *Sheffield Hallam University*, preprint, 2023.
- [3] M. Bianchi et al., "Vibration transmissibility and damping behaviour for auxetic and conventional foams," *University of Bristol, Technical Report*, 2013.
- [4] L. Yang et al., "Mechanical properties of 3D-printed lattice structures: Experimental and simulation study," *Additive Manufacturing*, vol. 23, pp. 505–515, 2018.
- [5] S. de la Rosa, P. F. Mayuet, J. R. Méndez Salgueiro, and L. Rodríguez-Parada, "Design of customized TPU lattice structures for additive manufacturing: Influence on the functional properties in elastic products," *Polymers*, vol. 13, no. 24, p. 4341, Dec. 2021, doi: 10.3390/polym13244341.
- [6] A. A. Pozniak, J. Smardzewski, and K. W. Wojciechowski, "Vibration transmissibility and damping behaviour of auxetic foams," *Smart Materials and Structures*, vol. 22, no. 8, p. 084009, Jul. 2013. [Online]. Available: <https://iopscience.iop.org/article/10.1088/0964-1726/22/8/084009>
- [7] T. Lim et al., "Auxetic metamaterials for impact and vibration mitigation: A review," *Smart Materials and Structures*, vol. 29, no. 9, p. 093001, 2020.
- [8] R. Lakes, "Foam structures with a negative Poisson's ratio," *Science*, vol. 235, no. 4792, pp. 1038–1040, 1987.
- [9] Y. Pu, S. Zheng, X. Hu, S. Tang, and N. An, "Robotic skins inspired by auxetic metamaterials for programmable bending of soft actuators," *Materials & Design*, vol. 246, p. 113334, Oct. 2024.
- [10] D. Chowdhury, Y.-E. Park, I. Jung, and S. Lee, "Characterization of exterior parts for 3D-printed humanoid robot arm with various patterns and thicknesses," *Polymers*, vol. 16, no. 7, p. 988, Apr. 2024.
- [11] M. Kang and S. Pyo, "Auxetic mechanical metamaterials for resistive tactile sensors: a review," *Advances in Physics: X*, vol. 10, no. 1, p. 2572830, Oct. 2025.
- [12] M. F. Simons, K. M. Digumarti, A. T. Conn, and J. Rossiter, "Tiled auxetic cylinders for soft robots," presented at the 2nd IEEE Int. Conf. Soft Robotics (RoboSoft), Seoul, South Korea, Apr. 2019, pp. 62–67.
- [13] A. A. Pozniak, J. Smardzewski, and K. W. Wojciechowski, "Computer simulations of auxetic foams in two dimensions," *Smart Materials and Structures*, vol. 22, no. 8, p. 084009, 2013.
- [14] L. Scetta, D. Tranchida, G. Malucelli, and D. Auhl, "Strain induced strengthening of soft thermoplastic polyurethanes," *Polymer Testing*, vol. 99, p. 107212, 2021.